ADVANCED FUNCTIONAL MATERIALS

FULL PAPER

DOI: 10.1002/adfm.200701150

Intramolecular Donor–Acceptor Regioregular Poly(3-hexylthiophene)s Presenting Octylphenanthrenyl-Imidazole Moieties Exhibit Enhanced Charge Transfer for Heterojunction Solar Cell Applications**

By *Yao-Te Chang, So-Lin Hsu, Guan-Yu Chen, Ming-Hsin Su, Thounaojam Avinash Singh, Eric Wei-Guang Diau,* and *Kung-Hwa Wei**

Intramolecular donor–acceptor structures prepared by covalently binding conjugated octylphenanthrenyl-imidazole moieties onto the side chains of regioregular poly(3-hexylthiophene)s exhibit lowered bandgaps and enhanced electron transfer compared to the parent polymer, e.g., conjugation of 90 mol% octylphenanthrenyl-imidazole moieties onto poly(3-hexylthiophene) chains reduces the optical bandgap from 1.91 to 1.80 eV, and the electron transfer probability is at least twice as high as that of pure poly(3-hexylthiophene) when blended with [6,6]-phenyl-C_{61}-butyric acid methyl ester. The lowered bandgap and the fast charge transfer both contribute to much higher external quantum efficiencies, thus much higher short-circuit current densities for copolymers presenting octylphenanthrenyl-imidazole moieties, relative to those of pure poly(3-hexylthiophene)s. The short-circuit current density of a device prepared from a copolymer presenting 90 mol% octylphenanthrenyl-imidazole moieties is 13.7 $mA \cdot cm^{-2}$ which is an increase of 65% compared to the 8.3 $mA \cdot cm^{-2}$ observable for a device containing pure poly(3-hexylthiophene). The maximum power conversion efficiency of this particular copolymer is 3.45% which suggest that such copolymers are promising polymeric photovoltaic materials.

1. Introduction

The development of conjugated polymers that possess extended delocalized π-electron systems and can be used in organic optoelectronic devices has been an area of extensive investigation, with earlier studies focusing on solar cell devices that are based on bulk heterojunctions of conjugated polymers.[1–7] Recently, research into conjugated polymers containing electron donor–acceptor pairs has become quite active,[8] because such materials exhibit unusual optical, electrical, and electronic properties. There are two kinds of donor–acceptor systems: intermolecular donor–acceptor systems, which are usually encountered in bulk heterojunction solar cells for instance, and intramolecular donor–acceptor systems, which enhance the rate of charge transfer within molecules or polymers.[8,9] As for intermolecular donor–acceptor systems like bulk heterojunction polymer solar cells; they are prepared using a thin film of an electron-donating conjugated polymer and an electron-accepting species that can either be another polymer or a set of nanoparticles.[8]

Intramolecular donor–acceptor systems typically consist of electron donating groups (e.g., conjugated polymers or small conjugated molecules), a bridge (e.g., another conjugated group or a long alkyl chain), and electron acceptors.[9] The photochemical and photophysical properties of such molecules or polymers depend on the kinetics of the excited-state processes that occur after absorption of a photon. After photoexcitation, the generated excitons are stabilized and further separated because of the extended conjugation length, and the electrons are subsequently transferred from the donors to the acceptors very rapidly.[9] Understanding of how excited states behave as a function of time is a significant challenge in designing novel molecules for solar cell applications. Typically, femtosecond time-resolved photoluminescence spectroscopy is used to obtain such information.[10] Two models for the intramolecular charge transfer process have been proposed: a twisted and a planar intramolecular charge transfer model. Because the charge transfer rate is higher for planar intramolecular charge transfers than it is for twisted intramolecular charge transfers,[9a] the charge separation process after photoexcitation will be more efficient if the introduction of

[*] Prof. K. H. Wei, Y. T. Chang, S. L. Hsu, G. Y. Chen, M. H. Su
Department of Materials Science and Engineering, National Chiao Tung University 1001 Ta Hsueh Road, Hsinchu, 30049 (Taiwan ROC)
E-mail: khwei@mail.nctu.edu.tw
Dr. T. A. Singh, Prof. E. W. G. Diau
Department of Applied Chemistry and Institute of Molecular Science
National Chiao Tung University
1001 Ta Hsueh Road, Hsinchu, 30049 (Taiwan ROC)

[**] We are grateful for financial support provided by the National Science Council through Project NSC 95-2120-M-009-007. We thank Hsu-Shen Wang for assistance with the synthesis of devices and Chen-Chia Chen for assistance with the study of devices discussed in this paper. Supporting Information is available online from Wiley InterScience or from the author.

ADVANCED FUNCTIONAL MATERIALS

electron-acceptor groups into the polymer side chains occurs in a coplanar manner. Moreover, the introduction of an electron-acceptor unit, usually a conjugated species that can absorb a different wavelength of sunlight, into the side chain of a conjugated polymer can widen the range of wavelengths of light that is absorbed. Therefore, conjugated polymers that contain side chain-tethered conjugated acceptor moieties do not only absorb light more effectively (multiple absorptions) but also exhibit an enhanced charge transfer ability, both of which are desirable properties in photovoltaic applications.[11] There are three methods for introducing electron acceptors into polymer structures: The first method is the introduction of C_{60} pendent functionalized groups as side chains of the polymer which consequently enhance the charge transfer. Unfortunately, C_{60} groups absorb very little light and tend to destroy the ability of the polymeric chains to crystallize, leading to lower power conversion efficiencies.[12] The second method involves the synthesis of panchromatic conjugated polymers that contain alternating donor–acceptor units in the main chains.[11] However, with this approach, the availability of suitable monomers becomes a very critical issue because it is an extremely difficult task to purify them. The third method is the incorporation of electron-withdrawing moieties as side chains that exist in conjugation with and coplanar to the polymeric main chains, which are the electron donors. This method has the additional advantage of allowing charge separation through sequential transfer of electrons from the main chains to the side chains and then to [6,6]-phenyl-C_{61}-butyric acid methyl ester (**PCBM**).

Polythiophene derivatives are among the most promising materials for solar cell applications because of their excellent light absorption and electron conductivity. Polymer solar cells containing blends of poly(3-hexylthiophene) and **PCBM** have been studied in depth and recent reports described power conversion efficiencies of ca. 4% under standard solar conditions (AM 1.5G, 100 mW · cm^{-2}, 25 °C).[13–18] To further improve the power conversion efficiencies of these heterojunction polymer solar cells, we designed a conjugated donor–acceptor polymer comprising poly(3-hexylthiophene) (**P3HT**) as the donor and side chain-tethered octylphenanthrenyl-imidazole groups as acceptors. In such systems, the charge transfer rate of the side chain-tethered octylphenanthrenyl-imidazole polymer is improved and the bandgap is lowered as a result of the increase in effective conjugation length. The extent of the reduction in the bandgap of these polymers, however, will depend on the effective conjugation length of the system, which is sometimes reduced through steric hindrance.[9c,9d] Previously, we synthesized poly(3-octylthiophene)s (**P3OT**) containing phenanthrenyl-imidazole moieties that did not exhibit good solubility because of their rigid chemical structures.[19] In the present study, we chose **P3HT** because the power conversion efficiency of a device incorporating **P3HT** and **PCBM** was higher than that of a device containing **P3OT** and **PCBM**. The two octyl chains in the phenanthrenyl-imidazole moiety were introduced to improve the solubility of the polymers. Scheme 1 displays the synthetic approach towards 2,5-dibromo-3-hexylthiophene and the planar phenanthrenyl-imidazole moiety-tethered thiophene monomer. We expected that the presence of octylphenanthrenyl-imidazole moieties conjugated onto the thiophene units would enhance the charge transfer rate of the polythiophene, with the octyl substituents improving the solubility of the polymer derivatives. Scheme 2 illustrates the copolymerization of 2,5-dibromo-3-hexylthiophene **M1** and 2-(2,5-dibromothiophen-3-yl)-6,9-dioctyl-1-phenyl-1*H*-phenanthro[9,10-*d*]imidazole monomer **M2**, performed using a Grignard metathesis approach. We also used a Grignard metathesis method to prepare **P3HT** for control experiments, i.e., the comparison of device performance of **P3HT** devices with that of devices prepared from our synthesized copolymers.

2. Results and Discussion

The regioregularity of the polymers was determined from ^{1}H NMR spectra, analyzing the ratio of the area below the peak at 6.98 ppm to the area of all peaks within the range of 6.98 to 7.04 ppm. Because of only one signal at 6.98 ppm being present in the spectra of **P3HT** and **P91**, with no other peaks nearby, we believe that these polymers possess an almost complete head-to-tail configuration (i.e., regioregularity close to 100%).[20] Due to the bulky octylphenanthrenyl-imidazole on one side of the thiophene monomers, the selectivity of these monomers during the grinard reaction becomes very high and the reaction first takes place at the bromide on the 5-position then at the bromide on the 2-position. Hence, the regioregularity of **P91** obtained was very high after polymerization. In the NMR spectrum of **P91** the peak at 6.73 ppm (CH proton of the thiophene ring) is absent, while broad peaks at 8.4–8.9 (CH protons of the phenanthrenyl group), 7.2–8.2 (CH protons on the phenyl group), and 0.8–3.0 ppm (octyl and hexyl chain protons) confirm that copolymers of **M1** and **M2** were formed. Details of the ^{1}H NMR spectra of all synthesized polymers are presented in Supporting Information Figure S1.

Table 1 displays molecular weights, degradation temperatures, and glass transition temperatures of all copolymers synthesized. The number molecular weights (M_n) of our polymers range from 8.9 to 13.5 kg · mol^{-1}, with polydispersity indices (PDI) ranging from 1.20 to 1.56. The thermal degradation temperature decreased upon increasing the content of octylphenanthrenyl-imidazole moieties because of the introduction of the octyl chains. The glass transition temperature of **P91** was not detectable, whereas it was measured to be 54.8 °C for **P3HT**.

Figure 1 displays UV–Vis spectra of obtained polymers in the solid state (thin films). The dihedral angle between the plane of octyl-phenanthrenyl-imidazole and that of thiophene is 82.13° as determined by molecular modeling (Chem. 3D, see supporting information, Figure S2.). Therefore, the small peak at 270 nm is caused by the presence of conjugated phenanthrenyl-imidazole moieties that are not fully coplanar with the polythiophene chains due to some steric hindrance. π-π^*

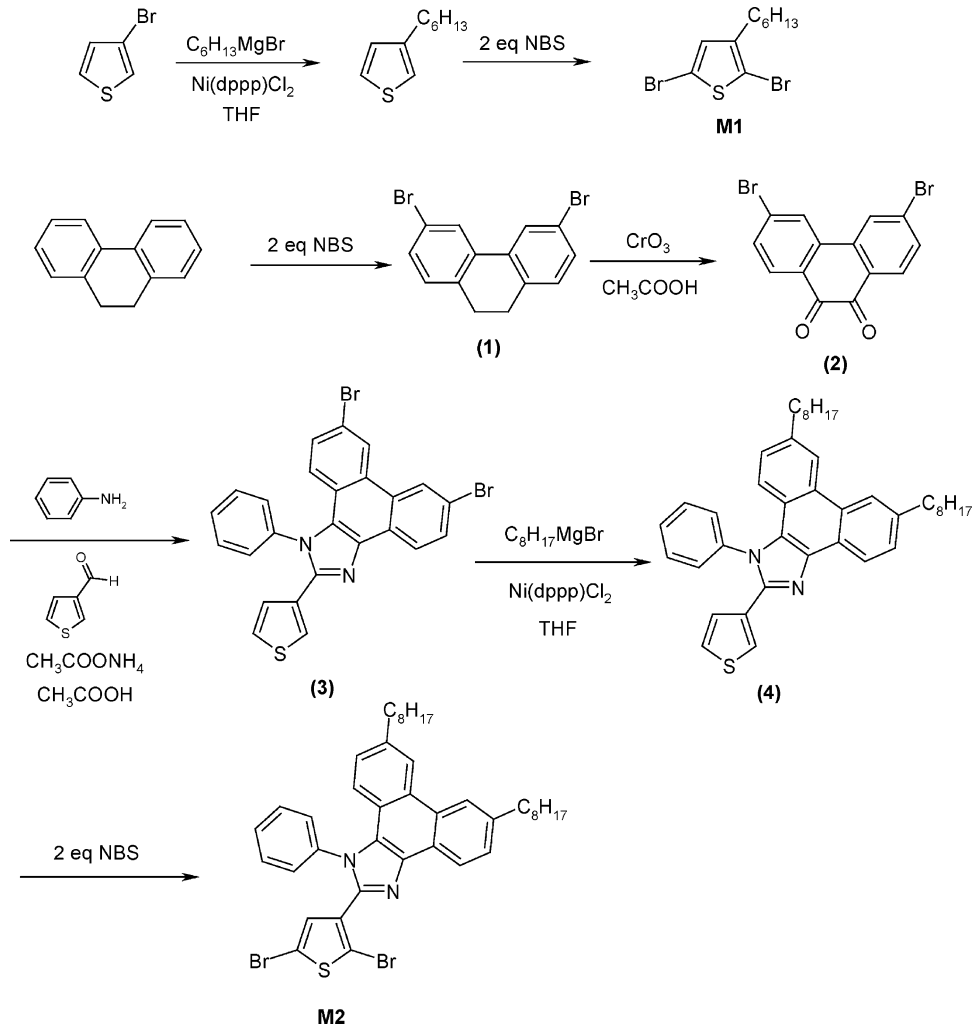

Scheme 1. Synthesis of **M1** and **M2**. NBS: *N*-bromosuccinimide.

transitions are responsible for the highest wavelength absorptions (λ_{max}) that occur at ca. 510 nm and 550 nm for **P3HT** and **P91** thin films, respectively.[21] This data indicates that the optical bandgap of the **P91** copolymer is lower than that of pure **P3HT**. Table 2 lists absorption maxima and optical bandgaps of all synthesized polymers. Conjugation of 90 mol% of octylphenanthrenyl-imidazole moieties with the polythiophene chains led to the optical bandgap being reduced from 1.91 to 1.80 eV, which confirms that the presence of the octylphenanthrenyl-imidazole moieties to some extent increased the effective conjugation length of the polythiophene main chain.[22] Cyclic voltammograms of the polymers also show the same phenomenon of the bandgap of the copolymers being reduced with increasing mole fraction of octylphenanthrenyl-imidazole moieties, despite the different absolute values (see Table S1 in the supporting information).

Figure 2 displays photoluminescence (PL) spectra of the polymer films, recorded with an excitation wavelength of 440 nm. The PL of the octylphenanthrenyl-imidazole-containing copolymers films is quenched dramatically compared to that of pure **P3HT**, with the degree of quenching increasing with an increasing number of phenanthrenyl-imidazole units in the copolymer. This finding suggests that photoinduced charge transfer occurred when the polymers were photoexcited. The charge transfer from the photoexcited polythiophene backbone to the electron-withdrawing phenanthrenyl-imidazole side chains was sufficiently rapid to compete with radiative recombination of the excitons.[23]

Figure 3 displays the normalized fluorescence transients of **PCBM**, our novel polymers, and blends of the polymers with **PCBM**, with excitation (λ_{ex}) and emission wavelengths (λ_{em}) of 440 nm and 600 nm, respectively. The transient of **PCBM** alone exhibits the background signal only, while the transient of each polymer alone features a biphasic relaxation feature. The excited-state relaxation of the polymer is mainly due to de-excitation of the quasi-thermal self-trapping exciton (STE).[24] The fluorescence decay of pure **P91** was slower than that of pure **P3HT**, possibly due to less aggregation of **P91** molecules

ADVANCED FUNCTIONAL MATERIALS

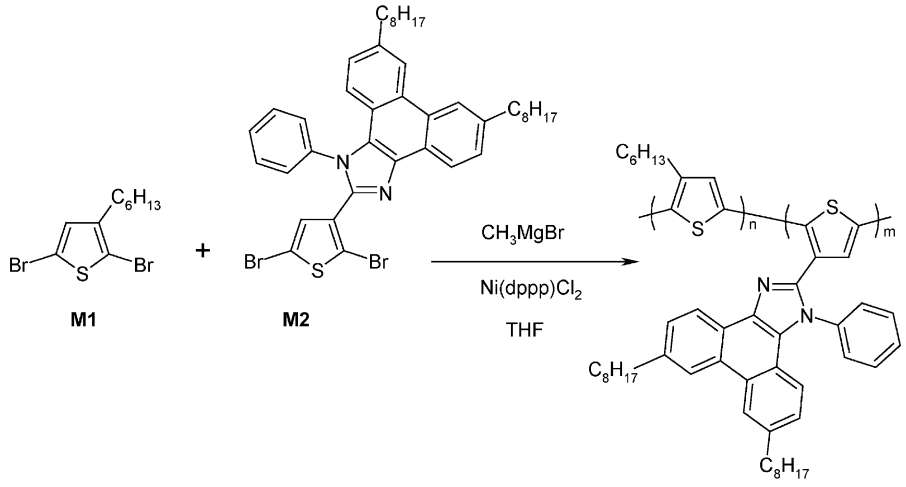

Polymer molar ratio	P3HT	P28	P46	P64	P82	P91
Molar fraction of **M1**	100%	80%	60%	40%	20%	10%
Molar fraction of **M2**	0	20%	40%	60%	80%	90%

Scheme 2. Grignard metathesis polymerization of **M1** and **M2.** THF: tetrahydrofuran.

in the film, which is a result of the steric effect of the bulky and conjugated octylphenanthrenyl-imidazole side groups. In both cases the fluorescence decay of a blend of the polymers with **PCBM** was faster than that of the individual polymer. Although the transients were quenched substantially when the polymers were blended with **PCBM**, the biphasic feature was retained in both cases. This phenomenon can be observed for MEHPPV (poly[2-methoxy-5-(2′-ethyl-hexyloxy)-1,4-phenylene vinylene]) and **PCBM**,[25] with the shortening of the lifetime being rationalized in terms of a rapid electron transfer resulting from the dissociation of the S_1 exciton of the polymer when a **PCBM** molecule is present in the vicinity of the polymer exciton. The fluorescence transients were thus fitted with two decay components according to a parallel kinetic model.[26] In the Supporting Information, we provide fluorescence decay data and kinetic fits for both polymers and their blends with **PCBM** at $\lambda_{em} = 600$, 620, and 660 nm ($\lambda_{ex} = 440$ nm). Each transient was deconvoluted into two components with time constants in the femtosecond and picosecond domain.

In the study of the fluorescence decay of polymer only samples, the single mode responsible for de-excitation is quenching, while in the case of blends of polymers with **PCBM** an additional de-excitation pathway is feasible due to electron transfer between the donor (polymer) and the acceptor (**PCBM**). Thus, the average rate constant of the pure polymer is considered to be k_q (the quenching rate constant), while that of the blend of polymers with **PCBM** equals the total rate constant, k_T, which includes both quenching rate and electron transfer rate constants. Therefore, it is feasible to evaluate the

Table 1. Molecular Weights and Thermal Properties of Synthesized Polymers.

Polymer	M_n [$\times 10^4$ g·mol^{-1}]	M_w [$\times 10^4$ g·mol^{-1}]	PDI [a.u.]	T_g [°C]	T_g [°C] [a]
P3HT	1.35	1.57	1.20	54.8	387.9
P28	1.10	1.56	1.46	71.4	382.4
P46	1.05	1.44	1.47	[b]	367.1
P64	0.98	1.46	1.48	[b]	332.4
P82	0.90	1.39	1.54	[b]	321.2
P91	0.89	1.38	1.56	[b]	313.3

[a] Temperature at which 5 wt% of the initial mass were lost. [b] Glass transition temperature was not observed.

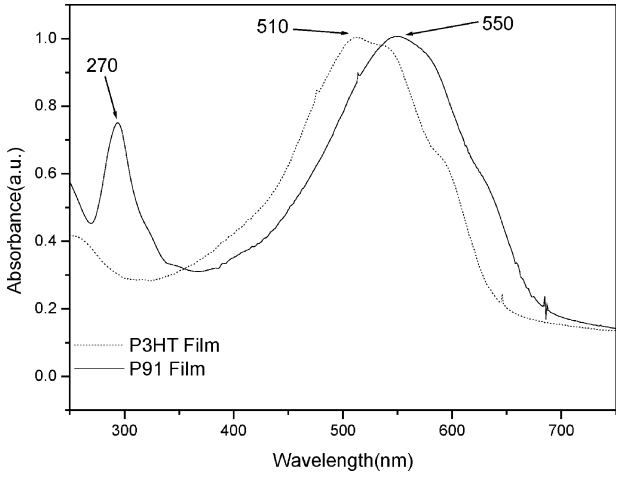

Figure 1. UV-Vis spectra of **P3HT** and **P91** in the solid state.

Table 2. UV-Vis Absorption Peaks and Optical Bandgaps of Synthesized Polymers.

Polymer	λ_{max}(solution) [nm]	λ_{max}(film) [nm]	bandgap [eV]
P3HT	439	510 (544, 595)	1.91
P28	445	522 (550, 600)	1.88
P46	451	530 (611)	1.86
P64	460	538 (628)	1.85
P82	466	546 (630)	183
P91	470	550 (634)	1.80

rate constant of the electron transfer process (k_{ET}) from the average rate constants of the polymers and the blend of the polymers with **PCBM**. Table 3 lists the average rate constants of the polymers (k_q) as well as those of the blends of polymers with **PCBM** (k_T), and the net electron transfer rate constants ($k_{ET} = k_T - k_q$). The ratio of k_{ET} to k_q provides a comparison between the two different pathways of de-excitation: electron transfer vs. quenching. The k_{ET}: k_q ratios at 600 nm are 1.45 and 3.46 for **P3HT**/**PCBM** and **P91**/**PCBM**, respectively, which means that a comparatively higher electron transfer probability exists in **P91** rather than **P3HT**, if blended with **PCBM**. Even at the longer emission wavelengths of 620 and 660 nm electron transfer was still much more favored in **P91** than **P3HT** (ratios of 1.67 vs. 0.31 and 1.04 vs. 0.31, respectively).

The photophysics of devices that incorporate the synthesized copolymers can be determined by examining their external quantum efficiencies. Figure 4 displays the external quantum efficiencies (EQE) of polythiophene side chain-tethered octylphenanthrenyl-imidazole/**PCBM** devices. EQE values were calibrated by using a reference cell and were divided by a mismatch factor of 1.34. The absolute EQE values of **P91** were at least 20% higher than that of self-made **P3HT** ($M_n \cong 13{,}500$) at wavelengths in the range 400–650 nm. When compared in more detail, the EQE value of the **P91** device at an incident wavelength of 460 nm is 73%, which is an increase of more than 40% compared to the **P3HT** device

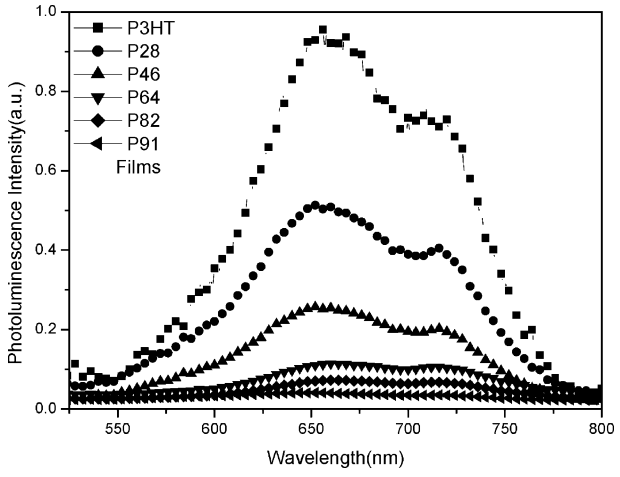

Figure 2. Photoluminescence (PL) spectra of synthesized polymers in the solid state. Spectra are normalized to the number of absorbed photons.

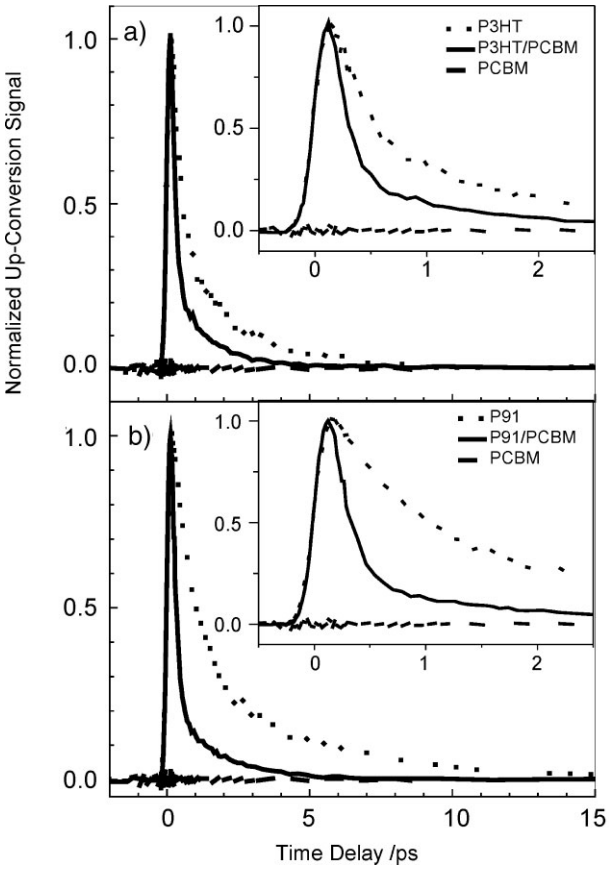

Figure 3. Normalized fluorescence transients of a) **P3HT** and b) **P91** coated on quartz. λ_{ex} and λ_{em} are 440 and 600 nm, respectively. The dotted curves represent the normalized transients of the polymer alone, the solid and the dashed curves correspond to those of polymer and **PCBM** blend and **PCBM** alone, respectively. The insets show the same transients at a shorter time range.

(EQE = 52%). The maximum EQE values of **P91** and **P3HT** devices at 400 nm excitation were 83% and 56%, respectively, which equals a 48% increase from the former to the latter. Even at much longer wavelengths (i.e., 640 nm) the EQE improved from 14% for the **P3HT**-based device to 47% for the **P91**-containing device — a twofold increase. This result indicates that introduction of octylphenanthrenyl-imidazole moieties into a polythiophene backbone can improve the light absorption of resulting heterojunction copolymer/**PCBM** devices.

Figure 5 displays the photocurrents measured for diodes with an overall structure of ITO/PEDOT:PSS/polymer: **PCBM**(1:1, w/w)/Ca/Al which were illuminated at AM 1.5G and 100 mW · cm^{-2}, as well as the dark currents measured for self-made **P3HT**/**PCBM** and **P91**/**PCBM** blends. As can be seen from the graph, the short-circuit current density (J_{sc}) increased upon increasing the content of octylphenanthrenyl-imidazole moieties, probably as a consequence of enhanced light absorption at longer wavelengths due to the extended conjugation and the fast charge transfer rate of the copolymers.[27] Table 4 lists short-circuit current densities,

ADVANCED FUNCTIONAL MATERIALS

Table 3. Rate constants for the polymer, its blend with **PCBM**, and electron transfer for **P3HT** and **P91** at different wavelengths.

λ [nm]	P3HT				P91			
	k_q [s^{-1}]	k_T [s^{-1}]	k_{ET} [s^{-1}]	k_{ET}/k_q [a.u.]	k_q [s^{-1}]	k_T [s^{-1}]	k_{ET} [s^{-1}]	k_{ET}/k_q [a.u.]
600	1.1×10^{12}	2.7×10^{12}	1.6×10^{12}	1.45	5.2×10^{11}	2.3×10^{12}	1.8×10^{12}	3.46
620	7.6×10^{11}	1.0×10^{12}	2.4×10^{11}	0.31	4.5×10^{11}	1.2×10^{12}	7.5×10^{11}	1.67
660	4.7×10^{11}	6.2×10^{11}	1.5×10^{11}	0.31	2.3×10^{11}	4.7×10^{11}	2.4×10^{11}	1.04

open-circuit voltages, and power conversion efficiencies of the heterojunction polymer solar cells, whereby short-circuit current density values were obtained after dividing the measured J_{sc} by a mismatch factor of 1.34. Worth mentioning is that the short-circuit current density of the device containing the copolymer with 90 mol% octylphenanthrenyl-imidazole, **P91**, was 13.7 $mA \cdot cm^{-2}$ which is an improvement of 65% from the 8.3 $mA \cdot cm^{-2}$ measured for the device containing pure poly(3-hexylthiophene). This calibrated short-circuit current density for the **P91** device, 13.7 $mA \cdot cm^{-2}$, is reasonably close to the empirical value of 13.4 $mA \cdot cm^{-2}$ which was obtained by integrating the current density-wavelength curves (see supporting information, Figure S3). Therefore, the short-circuit current density values of our devices are quite reasonable. We performed two control experiments using i) self-made **P3HT** of similar molecular weight ($M_n \cong 13{,}500$) to that of **P91** ($M_n \cong 8{,}900$),[28] and ii) commercially available high molecular weight **P3HT** ($M_n \cong 33{,}000$). Devices thereof were subjected to the same processing conditions as **P91.**

Upon experiencing a similar thermal treatment like **P91**, the power conversion efficiency of the device prepared from self-made low molecular weight **P3HT** and **PCBM** was 2.26%, which is in agreement with values reported in the literature,[28a] whilst that of a device prepared using commercially available **P3HT** and **PCBM** was 2.9%, which is lower than its nominal value of ~4% (Fig. 5). The performance of self-made **P3HT/PCBM**, commercial **P3HT/PCBM**, and **P91/PCBM** devices, which all experienced the same thermal treatment, was

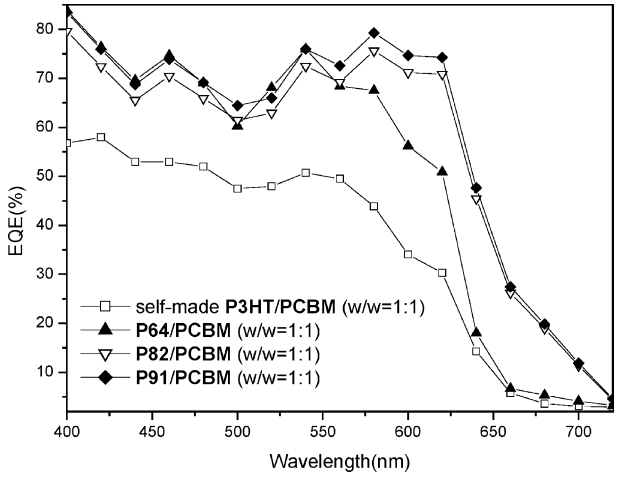

Figure 4. External quantum efficiencies of copolymer/**PCBM** solar cells.

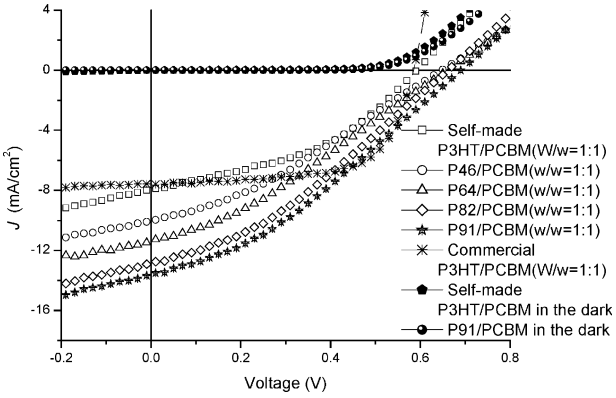

Figure 5. Current density-voltage characteristics of illuminated (AM 1.5G, 100 $mW \cdot cm^{-2}$) polymer solar cells incorporating self-made **P3HT**, **P64**, **P82**, **P91** and **PCBM**.

compared. A thermal treatment of 120 °C for 30 min seems to be optimal for the **P91** blend, but this is not the case for the self-made **P3HT/PCBM** blend or the commercial **P3HT/PCBM** blend. Consequently, the **P91/PCBM** device has a higher power conversion efficiency than that of self-made **P3HT/PCBM** or commercial **P3HT/PCBM** devices when this particular thermal treatment is used, but this does not necessarily need to be the case for other thermal treatment conditions. However, the key point is that despite the much lower molecular weight of polythiophene-imidazole copolymers compared to that of commercial **P3HT**, the power conversion efficiency of the **P91/PCBM** device is close to that of an optimal commercial **P3HT/PCBM** device(~4%), which

Table 4. Photovoltaic properties of the polymer solar cells.

	short-circuit current density (J_{sc}) [$mA \cdot cm^{-2}$] [a]	open-circuit voltage (V_{oc}) [V]	fill factor (FF) [%]	power conversion efficiency (PCE) [%]
Self-made				
P3HT	8.3	0.6	42.0	2.26
P46	10.1	0.64	37.4	2.42
P64	11.7	0.66	34.2	2.63
P82	13. 0	0.67	33.1	2.85
P91	13.7	0.68	37.2	3.45
Commercial				
P3HT	7.6	0.58	65.9	2.90

[a] The short-circuit current density values were divided by a mismatch factor of 1.34.

indicates the advantage of using this particular molecular architecture. Because of the increased short-circuit current density that occurred when the octylphenanthrenyl-imidazole content increased, the current density–voltage characteristics of our solar cell devices suggest that charge transport occurred from the photoexcited polythiophene backbone through the octylphenanthrenyl-imidazole moieties and **PCBM** to the electrode.[13,29] Evidence that charge transfer occurs from the photoexcited polythiophene backbone to the electron-withdrawing phenanthrenyl-imidazole was provided by the photoluminescence quenching data shown in Figure 2, while the data shown in Table 3 (fluorescence decay study) indicates that when blended with **PCBM**, an electron transfer from **P91** to **PCBM** occurs. By analyzing the sequence of these ttwo events, it is feasibly that a stepwise electron transfer from the polythiophene main chain to the imidazole to **PCBM** occurs. The possible mechanism of the charge transport can be explained by the following sequential events: Initially, photogenerated electrons are withdrawn from the photoexcited polythiophene backbone by the octylphenanthrenyl-imidazole moieties whilst holes are being retained within the polythiophene. Then, these electrons are being transferred to the nearby **PCBM**, followed by transfer to another **PCBM** by tunneling through **P91**, eventually reaching the Ca/Al electrode. In the meantime the holes are transported along the photoexcited polythiophene backbone and reached the **P91** molecules by tunneling through **PCBM**. Eventually, the holes pass through the PEDOT to reach the ITO electrode. The open circuit voltage (V_{oc}) increased from 0.60 V for the **P3HT/PCBM** device to 0.68 V for the **P91/PCBM** heterojunction device. The open circuit voltage of a polymer heterojunction cell is usually proportional to the difference between the lowest unoccupied molecular orbital (LUMO) of the electron acceptor and the highest occupied molecular orbital (HOMO) of the electron donor,[30] but it is also influenced by many other factors, e.g., solvent effects.[31] From the cyclic voltammogram shown in Supporting Information Table S1 it can be seen that the HOMO of **P91** (−4.65 eV) is slightly higher than that of **P3HT** (−4.75 eV), with the difference being 0.1 eV. The solubility of **P91** in dichlorobenzene, however, is still much less than that of **P3HT**, despite the fact that two octyl chains were added to the phenanthrenyl-imidazole in order to improve its solubility.[32] As for the **P91/PCBM** device, it appears that the effect of the copolymers becoming less miscible with **PCBM** at high octylphenanthrenyl-imidazole content,[31] dominated over the effect of the decrease in difference between LUMO of the electron acceptor (**PCBM)** and HOMO of the electron donor (**P91**), which results in a slightly higher V_{oc} value than that of the **P3HT/PCBM** device. This is because the octylphenanthrenyl-imidazole moieties can form π-π stacks among themselves and are therefore not quite as miscible with **PCBM**. The two octyl chains on the imidazole groups also increase the spatial distance between the octylphenanthrenyl-imidazole moiety and **PCBM**. Hence, the *Voc* of **the P91/PCBM** device was higher than that of the **P3HT/PCBM** device. Nevertheless, fill factors remained low as a result of the devices maintaining large series resistances and low shunt resistances.[33] Compared to our findings in previous studies, however, fill factors slightly improved when dioctyl groups were incorporated into the phenanthrenyl-imidazole moieties, because of the improved solubility. Figure 6 displays atomic force microscopy images of self-made **P3HT/PCBM** and **P91/PCBM** (1:1, w/w) films. The root-mean-square roughness of the **P91/PCBM** film (2.26 nm), was twice as high as that of the **P3HT/PCBM** film (1.13 nm), and the structure of **P91/PCBM** appeared to be better organized than that of **P3HT/PCBM**. We suspect that the rough surface may effectively reduce the charge-transport distance while at the same time providing a nanoscaled texture that further enhances internal light absorption.[16b,34] Consequently, the power conversion efficiency increased dramatically, i.e., to 3.45% for **P91**, which is presumably the result of a lower bandgap and an enhanced electron transfer as well as a more organized structure in the active layer of the device.

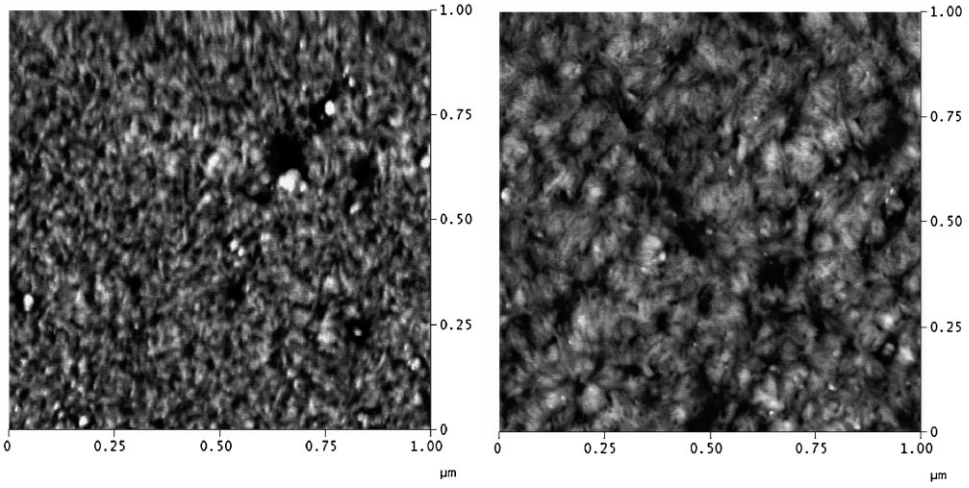

Figure 6. Atomic force microscopy images of a) self-made **P3HT/PCBM** and b) **P91/PCBM** films.

ADVANCED FUNCTIONAL MATERIALS

3. Conclusions

We prepared a new family of regioregular poly(3-hexylthiophene) copolymers, which present octylphenanthrenyl-imidazole side chains in conjugation with the main chain and that exhibit lowered bandgaps. The reduction in bandgap energy in conjunction with photoluminescence quenching indicates that a rapid charge transfer occurrs in the device from the photoexcited polythiophene backbone, through the octylphenanthrenyl-imidazole moieties, to the **PCBM** units. Ratios of net electron transfer rate constant to quenching rate constant at different wavelengths were much higher for the copolymer incorporating 90 mol% octylphenanthrenyl-imidazole moieties blended with **PCBM** than for **P3HT/PCBM**, indicating that the electron transfer probability of the former is greatly favored over that of the latter. The high external quantum efficiency of the device that incorporates the polythiophene-side-chain-tethered octylphenanthrenyl-imidazole results in a high short-circuit current density. And because of this high short-circuit current density as well as a more organized active layer structure obtained for octylphenanthrenyl-imidazole presenting regioregular poly(3-hexylthiophene)s, the power conversion efficiency is improved dramatically, i.e., to 3.45% for the copolymer containing 90 mol% octylphenanthrenyl-imidazole.

4. Experimental

Materials: Chemicals were purchased from Aldrich, TCI, or Lancaster. [6,6]-Phenyl-C_{61}-butyric acid methyl ester (**PCBM**) was purchased from Nano-C. Polyethylenedioxythiophene/ polystyrenesulphonate (PEDOT/PSS) was purchased from Baytron (P VP A1 4083).

Preparation of Monomers: Scheme 1 illustrates the synthetic route followed for the preparation of the monomers 2,5-dibromo-3-hexylthiophene (**M1**) and 2-(2,5-dibromothiophen-3-yl)-6,9-dioctyl-1-phenyl-1*H*-phenanthro[9,10-d]imidazole (**M2**). 6,9-Dibromo-1-phenyl-2-(thiophen-3-yl)-1*H*-phenanthro[9,10-d]imidazole (**3**) was isolated with 92% yield following the reaction of 3-thiophenecarboxaldehyde, phenanthrenequinone, aniline, ammonium acetate, and acetic acid. 6,9-Dioctyl-1-phenyl-2-(thiophen-3-yl)-1*H*-phenanthro[9,10-d]imidazole (**4**) was isolated in 80% yield from the reaction of compound **3** with octyl magnesium bromide and Ni(dppp)Cl_2 under reflux. 2-(2,5-Dibromothiophen-3-yl)-6,9-dioctyl-1-phenyl-1*H*-phenanthro[9,10-d]imidazole (**M2**) was isolated in 93% yield from the reaction between compound **2** and *N*-bromosuccinimide (NBS) [19]. Detailed synthetic procedures as well as characterization data are provided in the Supporting Information.

Preparation of Polythiophene Derivatives: All polymers were synthesized through Grignard metathesis polymerizations in tetrahydrofuran (THF), according to procedures similar to those described in the literature [20]. The Grignard metathesis polymerizations of 2,5-dibromo-3-hexylthiophene (**M1**) and 2-(2,5-dibromothiophen-3-yl)-1-phenyl-1*H*-phenanthro[9,10-d]imidazole (**M2**) are illustrated in Scheme 2. Detailed synthetic procedures and characterization data are provided in the Supporting Information.

Instrumentation: ^1H and ^{13}C NMR spectra were recorded on a Varian Unity-300 NMR spectrometer. Elemental analysis (EA) of the polymers was performed using a Heraeus CHN-OS Rapid instrument. Thermal gravimetric analysis (TGA) of the polythiophene derivatives was performed using a Du Pont TGA 2950 instrument operated at a heating rate of $10\,K \cdot min^{-1}$ under nitrogen flow. Differential scanning calorimetry (DSC) was performed on a Du Pont DSC 2010 instrument operated at a heating rate of $10\,K \cdot min^{-1}$ under nitrogen flow. Samples were heated from 30 to 200 °C, cooled to 20 °C, and then heated again from 30 to 200 °C. Glass transition temperatures (T_g) were determined from the second heating scans. UV–Vis spectra were measured using an HP 8453 diode array spectrophotometer. PL spectra were recorded using a Hitachi F-4500 luminescence spectrometer. Molecular weights of the polythiophene derivatives were determined via gel permeation chromatography (GPC) using a Waters chromatography unit interfaced to a Waters 2414 differential refractometer. Three 5 μm Waters styragel columns were connected in series in decreasing order of pore sizes (10^4, 10^3, and 10^2 Å); THF was the eluent and standard polystyrene samples were used for calibration. The redox behavior of each polymer was investigated by cyclic voltammetry using 0.1 M tetrabutylammonium hexafluorophosphate (n-Bu_4NPF_6) in acetonitrile as electrolyte. Cyclic voltammetry measurements were performed using a BAS 100 electrochemical analyzer, operated at a potential scan rate of $40\,mV \cdot s^{-1}$. In each case, a glassy disk carbon electrode coated with a thin layer of a polymer was used as the working electrode; a platinum wire as the counter electrode, and a silver wire as the quasi-reference electrode. All of the potentials quoted herein used Ag wire as the quasi-reference electrode. The electrochemical potential of Ag is −0.02 V vs. saturated calomel electrode (SCE). $E_{HOMO} = -E_{ox} - 4.4$ eV and $E_{LUMO} = -E_{red} - 4.4$ eV, where E_{ox} and E_{red} are the onset potentials (vs. SCE) of the oxidation and reduction peaks, respectively, and the value of 4.4 eV relates the SCE reference to the vacuum. The topography of **P3HT/PCBM** and **P91/PCBM** films was obtained by atomic force microscopy (AFM) using a Digital Instruments Nanoscope IIIa instrument at a scan rate of 1.0 Hz in tapping mode. AFM samples were prepared by spin-coating solutions of polymer/**PCBM** blends in dichlorobenzene on silica wafer substrates, followed by annealing at 120 °C for two hours in an oven.

Time-Resolved Photoluminescence Spectroscopy: Relaxation dynamics of the thin-film samples were studied using a femtosecond fluorescence up-conversion technique. The experimental details thereof are available elsewhere [26]. In brief, a fluorescence optically gated system (FOG100, CDP) was used in conjunction with a mode-locked Ti-sapphire laser (Mira900D, Coherent) pumped with a 10-W Nd:YVO4 laser (Verdi-V10, Coherent) to produce femtosecond pulses with a pulse width of 160 fs, a wavelength centered at 880 nm, and a repetition rate of 76 MHz. The frequency of the laser pulse was doubled using a non-linear crystal to obtain a pulse of 440 nm, which was used as excitation pulse, while the residual fundamental pulse was used as an optical gate. A dichroic beam splitter separated excitation beam and gate beam. The intensity of the excitation beam was appropriately attenuated using various neutral density filters while the plane of polarization was altered to maintain magic angle conditions (54.7°). The excitation beam was then focused onto a 1 mm rotating cell containing the solid thin-film samples. The emission was directed towards another non-linear crystal with the aid of a pair of parabolic mirrors. The gated pulse and the emission were focused on the BBO crystal to obtain maximum spatial overlap when the sum-frequency was generated. This sum-frequency signal was passed through an iris and band-pass filter to eliminate stray light, focused on a double-monochromator (DH10, Jobin Yvon) with a lens, and then detected with a photomultiplier (R1527P, Hamamatsu) which was connected to a computer-controlled photon-counting system. A temporal profile could be obtained by varying the delay between the gate and the excitation pulses via a stepping-motor translational stage.

Device Fabrication: Current density–voltage (J-V) measurements were performed using devices with a sandwich structure [ITO/PEDOT:PSS/polymer:**PCBM** (1:1, w/w)/Ca/Al]. The ITO-coated glass substrate was pre-cleaned and treated with oxygen plasma prior to use. The polymer/**PCBM** layers were spin-coated from their corresponding dichlorobenzene solutions ($20\,mg \cdot mL^{-1}$) at 1500 rpm. Having tried several other solvents such as toluene, chloroform, and tetrahydro-

furan, dichlorobenzene seems to be the best solvent to dissolve our polymers. The nominal thickness of polymer/**PCBM** layers was ca. 80 nm. The active layers of our devices were thermally annealed at 120 °C for 30 min prior to electrode deposition. Different thermal treatment conditions for the samples were trialed, i.e., samples were subjected to thermal annealing at 110 °C, 120 °C, and 150 °C for 30 min, respectively. Thermal treatment at 120 °C for 30 min was found to give optimal power conversion efficiency for the final devices. Using a base pressure below 1×10^{-6} torr, a layer of Ca (30 nm) was vacuum-deposited as the cathode followed by deposition of a thick layer of Al (100 nm) as the protecting layer. The effective area of one cell was 0.04 cm^2.

Device Performance Tests: Testing of the devices was performed under simulated AM 1.5G irradiation (100 $mW \cdot cm^{-2}$) using a xenon lamp-based Newport 66902 150 W solar simulator. A xenon lamp equipped with an AM 1.5G filter was used as the white light source and the optical power at the sample was 100 $mW \cdot cm^{-2}$ as detected by an OPHIR thermopie 71964. *J-V* characteristics were measured using a Keithley 236 electrometer. The spectrum of our solar simulator had a mismatch of less than 25%. The spectrum of the solar simulator was calibrated using a PV-measurement (PVM-154) mono-Si solar cell (NREL calibrated), and a Si photo diode (Hamamatsu S1133) was used to check the uniformity of the area exposed. The AM 1.5G (ASTM G173) light intensity was calibrated by thermopie and PV-measurement [35]. The mismatch factor (M) was 1.34, which was obtained by taking the PVM-154 as reference cell and devices of **P3HT/PCBM** and **P91/PCBM** as test cells and calculating the spectrum from 300 nm to 900 nm in steps of 10 nm (see supporting information Eq. 1). The PVM-154 was combined with a KG-5 filter (350 nm ~ 700 nm pass, Newport) to simulate a reference solar cell with spectral responsivity from 350 nm to 700 nm. Reported efficiencies are the averages obtained from four devices prepared on each substrate. External quantum efficiencies (EQE) were measured using a Keithley 236 instrument coupled with an Oriel Cornerstone 130 monochromator. The light intensity at each wavelength was calibrated using an OPHIR 71580 diode.

Received: October 5, 2007
Revised: March 12, 2008

[1] a) C. Ego, D. Marsitzky, S. Becker, J. Zhang, A. C. Grimsdale, K. Müllen, J. D. MacKenzie, C. Silva, R. H. Friend, *J. Am. Chem. Soc.* **2003**, *125*, 437. b) J. Pei, W. Yu, J. Ni, Y. Lai, W. Huang, A. J. Heeger, *Macromolecules* **2001**, *34*, 7241. c) F. Zhang, E. Perzon, X. J. Wang, W. Mammo, M. R. Andersson, O. Inganäs, *Adv. Funct. Mater.* **2005**, *15*, 745. d) O. Inganäs, M. Svensson, F. Zhang, A. Gadisa, N. K. Persson, X. Wang, M. R. Andersson, *Appl. Phys. A: Mater. Sci. Process.* **2004**, *79*, 31. e) M. Y. Chiu, U. S. Jeng, C. H. Su, K. S. Liang, K. H. Wei, *Adv. Mater.* **2008**, in press.

[2] J. H. A. Smits, S. C. J. Meskers, R. A. J. Janssen, A. W. Marsman, D. M. D. Leeuw, *Adv. Mater.* **2005**, *17*, 1169.

[3] G. Yu, J. Gao, J. C. Hummelen, F. Wudl, A. J. Heeger, *Science* **1995**, *270*, 1789.

[4] W. U. Huynh, J. J. Dittmer, A. P. Alivisatos, *Science* **2002**, *295*, 2425.

[5] K. M. Coakley, M. D. McGehee, *Chem. Mater.* **2004**, *16*, 4533.

[6] T. J. Savenije, J. E. Kroeze, X. Yang, J. Loos, *Adv. Funct. Mater.* **2005**, *15*, 1260.

[7] Y. Liu, M. A. Summers, C. Edder, J. M. J. Fréchet, M. D. McGehee, *Adv. Mater.* **2005**, *17*, 2960.

[8] a) C. J. Brabec, N. S. Sariciftci, J. C. Hummelen, *Adv. Funct. Mater.* **2001**, *11*, 15. b) S. C. Ng, H.-F. Lu, H. S. O. Chan, A. Fujii, T. Laga, K. Yoshino, *Adv. Mater.* **2000**, *12*, 1122. c) Z. Bao, Z. Peng, M. E. Galvin, E. A. Chandross, *Chem. Mater.* **1998**, *10*, 1201. d) S. Son, A. Dodabalapur, A. J. Lovinger, M. E. Galvin, *Science* **1995**, *269*, 376.

[9] a) T. Yoshihara, S. I. Druzhinin, K. A. Zachariasse, *J. Am. Chem. Soc.* **2004**, *126*, 8535. b) A. Escosura, M. V. Martínez-Díaz, D. M. G. T. Torres, *J. Am. Chem. Soc.* **2006**, *128*, 4112. c) E. H. A. Beckers, S. C. J. Meskers, A. P. H. J. Schenning, Z. Chen, F. Würthner, P. Marsal, D. Beljonne, J. Cornil, R. A. J. J. Janssen, *Am. Chem. Soc.* **2006**, *128*, 649. d) A. M. Ramos, S. C. J. Meskers, E. H. A. Beckers, R. B. Prince, L. Brunsveld, R. A. J. Janssen, *J. Am. Chem. Soc.* **2004**, *126*, 9630. e) D. M. Guldi, A. Swartz, C. Luo, R. Gómez, J. L. Segura, N. Martin, *J. Am. Chem. Soc.* **2002**, *124*, 10875. f) P. Samorí, X. Yin, N. Tchebotareva, Z. Wang, T. Pakula, F. Jäckel, M. D. Watson, A. Venturini, K. Müllen, J. P. Rabe, *J. Am. Chem. Soc.* **2004**, *126*, 3567. g) V. Lemaur, M. Steel, D. Beljonne, J.-L. Brédas, J. Cornil, *J. Am. Chem. Soc.* **2005**, *127*, 6077. h) M. L. Kirk, D. A. Shultz, E. C. Depperman, C. L. Brannen, *J. Am. Chem. Soc.* **2007**, *129*, **1937**. i) S. Handa, F. Giacalone, S. A. Haque, E. Palomares, N. Martin, J. R. Durrant, *Chem. Eur. J.* **2005**, *11*, 7440.

[10] W. J. E. Beek, M. M. Wienk, R. A. J. Janssen, *Adv. Funct. Mater.* **2006**, *16*, 1112.

[11] Z. Zhu, D. Waller, R. Gaudiana, M. Morana, D. Mühlbacher, M. Scharber, C. J. Brabec, *Macromolecules* **2007**, *40*, **1981**.

[12] a) Z. Tan, J. H. Hou, Y. J. He, E. Zhou, C. Yang, Y. F. Li, *Macromolecules* **2007**, *40*, 1868. b) A. Cravino, N. S. Sariciftci, *J. Mater. Chem.* **2002**, *12*, 1931. c) A. Cravino, G. Zerza, M. Maggini, S. Bucella, M. Svewnsson, M. R. Andersson, H. Neugebauer, N. S. Sariciftci, *Chem. Commun.* **2000**, *24*, 2487. d) A. Marcos Ramos, M. T. Rispens, J. C. Hummelen, R. A. J. Janssen, *Synth. Met.* **2001**, *119*, 171. e) F. Zhang, M. Svensson, M. R. Andersson, M. Maggini, S. Bucella, E. Menna, O. Inganäs, *Adv. Mater.* **2001**, *13*, 1871. f) A. Marcos Ramos, M. T. Rispens, J. K. J. Van Duren, J. C. Hummelen, R. A. J. Janssen, *J. Am. Chem. Soc.* **2001**, *123*, 6714. g) F. Giacalone, N. Martin, *Chem. Rev.* **2006**, *106*, 5136. h) X. Wang, E. Perzon, F. Oswald, F. Langa, S. Admassie, M. R. Andersson, O. Inganäs, *Adv. Funct. Mater.* **2005**, *15*, 1665. i) X. J. Wang, E. Perzon, J. L. Delgado, P. de la Cruz, F. Zhang, F. Langa, M. R. Andersson, O. Inganäs, *Appl. Phys. Lett.* **2004**, *85*, 5081.

[13] V. D. Mihaiketchi, H. Xie, B. D. Boer, L. J. A. Koster, P. W. M. Blom, *Adv. Funct. Mater.* **2006**, *16*, 699.

[14] J. Hou, Z. Tan, Y. Yan, Y. He, C. Yang, Y. F. Li, *J. Am. Chem. Soc.* **2006**, *128*, 4911.

[15] K. Sivula, Z. T. Ball, N. Watanabe, J. M. J. Fréchet, *Adv. Mater.* **2006**, *18*, 206.

[16] a) G. Li, V. Shrotriya, Y. Yao, Y. Yang, *J. Appl. Phys.* **2005**, *98*, 043704. b) G. Li, V. Shrotriya, J. Huang, Y. Yao, T. Moriarty, K. Emery, Y. Yang, *Nat. Mater.* **2005**, *4*, 864.

[17] T. Erb, U. Zhokhavets, G. Gobsch, S. Raleva, B. Stühn, P. Schilinsky, C. Waldauf, C. J. Brabec, *Adv. Funct. Mater* **2005**, *15*, 1193.

[18] I. Riedel, E. V. Hauff, J. Parisi, N. Martin, F. Giacalone, V. Dyakonov, *Adv. Funct. Mater.* **2005**, *15*, 1979.

[19] Y.-T. Chang, S.-L. Hsu, M.-H. Su, K.-H. Wei, *Adv. Funct. Mater.* **2007**, *17*, 3326.

[20] a) R. D. McCullough, R. D. Lowe, M. Jayaraman, D. L. Anderson, *J. Org. Chem.* **1993**, *58*, 904. b) M. C. Iovu, E. E. Sheina, R. R. Gil, R. D. McCullough, *Macromolecules* **2005**, *38*, 8649. c) E. E. Sheina, S. M. Khersonsky, E. G. Jones, R. D. McCullough, *Chem. Mater.* **2005**, *17*, 3317.

[21] A. R. Murphy, J. Liu, C. Luscombe, D. Kavulak, J. M. J. Fréchet, R. J. Kline, M. D. McGehee, *Chem. Mater.* **2005**, *17*, 4892.

[22] J. Roncali, *Chem. Rev.* **1997**, *97*, 173.

[23] F. Giacalone, J. L. Segura, N. Martin, M. Catellani, S. Luzzati, N. Lupsac, *Org. Lett.* **2003**, *5*, 1669.

[24] A. Matsuse, S. Takeucho, K. Yoshino, T. Kobayashi, *Chem. Phys. Lett* **1998**, *288*, 165.

ADVANCED FUNCTIONAL MATERIALS

[25] J. G. Müller, J. M. Lupton, J. Feldmann, U. Lemmer, M. C. Scharber, N. C. Sariciftci, C. J. Brabec, U. Scherf, *Phys. Rev. B* **2005**, *72*, 195208.
[26] L.-Y. Luo, C.-F. Lo, C.-Y. Lin, I.-J. Chang, E. W.-G. Diau, *J. Phys. Chem. B* **2006**, *110*, 410.
[27] C. Waldauf, P. Schilinsky, J. Hauch, C. J. Brabec, *Thin Solid Films* **2004**, *451-452*, 503.
[28] a) P. Schilinsky, U. Asawapirom, U. Scherf, M. Biele, C. J. Brabec, *Chem. Mater.* **2005**, *17*, 2175. b) W. Ma, J. Y. Kim, K. Lee, A. J. Heeger, *Macromol. Rapid Commun.* **2007**, *28*, 1776.
[29] A. Pivrikas, N. S. Sariciftci, G. Juška, R. Osterbacka, *Prog. Photovolt. Res. Appl.* **2007**, *15*, 677.
[30] M. C. Scharber, D. Mühlbacher, M. Kopper, P. Denk, C. Waldauf, A. J. Heeger, C. J. Brabec, *Adv. Mater.* **2006**, *18*, 789.
[31] J. Liu, Y. Shi, Y. Yang, *Adv. Funct. Mater.* **2001**, *11*, 420.
[32] C. Shi, Y. Yao, Y. Yang, Q. Pei, *J. Am. Chem. Soc.* **2006**, *128*, 8980.
[33] W. Ma, C. Yang, X. Gong, K. Lee, A. J. Heeger, *Adv. Funct. Mater.* **2005**, *15*, 1617.
[34] S. Berson, R. D. Bettignies, S. Bailly, S. Guillerez, *Adv. Funct. Mater.* **2007**, *17*, 1377.
[35] American Society for Testing and Materials (ASTM) standard G173, ''Standard Tables for Reference Solar Spectrum Irradiance: Direct Normal and Hemispherical on 37° Tilted Surface.''